Journal of Materiomics 11 (2025) 100887

Contents lists available at ScienceDirect

Journal of Materiomics

journal homepage: www.journals.elsevier.com/journal-of-materiomics/

Research paper

Poling-free relaxor-$PbTiO_3$ single crystals

Hwang-Pill Kim [a, 1, 2], Geon-Ju Lee [a, 1, 3], Ju-Hyeon Lee [a], Jae-Hyeon Cho [a, 4], Hye-Lim Yu [a], Woo-Seok Kang [a, 3], Joo-Hee Kang [c], Ho-Yong Lee [d], Wook Jo [a, *]

[a] Department of Materials Science and Engineering, Ulsan National Institute of Science and Technology (UNIST), Ulsan, 44919, Republic of Korea
[c] Department of Materials Analysis, Korea Institute of Materials Science, 797 Changwondaero, Seongsan, Changwon, Gyeongnam, 51508, Republic of Korea
[d] Department of Materials Science and Engineering, Sun Moon University, Asan, 31460, Republic of Korea

ARTICLE INFO

Article history:
Received 21 February 2024
Received in revised form
21 April 2024
Accepted 5 May 2024
Available online 29 May 2024

Keywords:
Piezoelectricity
Self-poling
$PbTiO_3$ single crystal
Relaxor ferroelectric

ABSTRACT

Relaxor-$PbTiO_3$ ferroelectric single crystals have drawn attention aiming at high-end piezoelectric applications thanks to their excellent piezoelectric properties. Like all the other ferroelectrics, relaxor-$PbTiO_3$ single crystals can only be piezoelectrically active upon being electrically poled. However, this poled state is thermally unstable, limiting their uses because of their relatively low depolarization temperature. Here, we show that a non-destructible permanent poled state can be realized in relaxor-$PbTiO_3$ single crystals by forming a 0−3 composite in the presence of charged mobile point defects. We demonstrate this on solid-state grown 0.71 $Pb(Mg_{1/3}Nb_{2/3})O_3$-0.29$PbTiO_3$ single crystals doped with Mn (Mn-PMNT) as a donor with well-aligned and dispersed boron-rich MgO-based inclusions (MBIs). Mn-$PMNT_{MBI}$ sharing [001] axis with arrayed MBIs were spontaneously polarized during cooling across the Curie temperature without an external electric field. The piezoelectric coefficient and dielectric permittivity of self-poled Mn-$PMNT_{MBI}$ crystals were as large as 90% of that achieved by a direct-current poling treatment at room temperature, and such poled state was reproducible against repeated thermal cycles. We expect that the poling-free high-performance piezoelectric relaxor-$PbTiO_3$ single crystals offer an avenue for piezoelectric-based devices by removing the working temperature limit as one of the inherent fundamental limitations.

1. Introduction

Piezoelectric materials have been widely employed for electromechanical transducers, leading to a number of novel applications, establishing a more than 30.9 billion USD-sized global market in 2022 [1] thanks to their electromechanical coupling. The piezoelectric-based electromechanical coupling is especially beneficial for high-speed, high-precision, and high-resolution devices [2−6] because it comes directly from cumulative atomic level interactions between structure and electrical dipole moments. However, these advantages have, conversely, been a major drawback for versatile uses of piezoelectricity for high-stroke actuators and wide-band transducers due to its relatively small inducible mechanical deformation (S_3 ~1%) and electromechanical coupling factor (k_{33} ~0.7).

The discovery of ultra-high piezoelectricity in relaxor-$PbTiO_3$ single crystals, represented by $Pb(Zn_{1/3}Nb_{2/3})O_3$−$PbTiO_3$ (PZNT) and $Pb(Mg_{1/3}Nb_{2/3})O_3$−$PbTiO_3$ (PMNT) [7,8] was a game changer for the piezoelectric industry because it has opened completely new applicational opportunities with their exceptionally large piezoelectric coefficients (d_{33} > 1500 pC/N, S_3 >1%) and electromechanical coupling (k_{33} > 0.9) [9,10]. Much efforts made to further enhance the electromechanical responses and stabilities of relaxor-$PbTiO_3$-based single crystals have been quite successful in alternating current poling [11], mechanical imprint effects [12,13], flattening energy landscapes [14,15], constructing phase boundaries [16], texturing [17−19] and precipitation hardening [20,21]. Especially it is worth noting that a recent discovery of Sm-doped PMNT demonstrates a giant piezoelectric coefficient (d_{33} ~4100 pC/N) [22].

* Corresponding author.
E-mail address: wookjo@unist.ac.kr (W. Jo).
Peer review under responsibility of The Chinese Ceramic Society.
[1] These authors contributed equally to this work.
[2] Current address: Maritime Technology Research Institute, Agency for Defense Development, Changwon 51682, Republic of Korea.
[3] Current address: Samsung Electro-Mechanics, 150 Maeyeong-ro, Yeongtong-gu, Suwon 16674, Gyeonggi-do, Republic of Korea.
[4] Current address: Samsung Electronics, 1-1, Samsungjeonja-ro, Hwaseong 18448, Gyeonggi-do, Republic of Korea.

https://doi.org/10.1016/j.jmat.2024.05.002

Despite the great success, however, stability and reliability during device operations have always been challenges because there is a clear trade-off between enhancing piezoelectric properties and securing their stability [3]. It is well-known that piezoelectricity peaks during symmetry-changing phase transformations with a sharp increase in compliance, *i.e.*, softening; thus, the room-temperature piezoelectric properties tend to become higher as a phase transformation temperature is in close proximity to room temperature [23]. This stability issue is no less significant than enhancing piezoelectricity, especially for practical applications, since even a self-heating inevitable with the hysteresis in electric-field-dependent polarization during operation could easily kill the piezoelectricity. Once depoled, the poled state cannot be recovered on-device. A complete repoling of failed piezoelements requires detaching from the working device, which is impractical in most cases. The strategies to manage this issue have, so far, been based mainly on engineering two parameters, *i.e.*, $T_{R\text{-}T}$ (rhombohedral-to-tetragonal phase transformation temperature) and E_c (coercive field). The state of the art is Mn-doped PMNT-based single crystals, which are featured by an elevated $T_{R\text{-}T}$ (>100 °C) and a relatively high E_c (>5 kV/cm) [24,25]. Nevertheless, the inherent instability issues in piezoelectricity remain unresolved.

An ultimate solution to resolving the stability issue will be to force the spontaneous polarization to be self-aligned along an intended specific orientation. The feasibility of this approach was demonstrated by He *et al.* [26] in a flux-grown Sn-doped PMNT single crystal. They claimed that a strong internal bias field was created *via* so-called symmetry-conforming defect dipoles [27], *i.e.*, reorientable defect complexes connecting reduced Sn^{2+} as an acceptor and charge-balancing oxygen vacancies. The so-called symmetry-conforming defect dipoles can, as the name implies, form a strong internal bias field only when the symmetry of the crystal is non-cubic. Once the macroscopic symmetry becomes cubic above Curie temperature (T_C), there is no driving force for the initially randomly oriented defect dipoles to be aligned with themselves. Likewise, there is no reason for an internal bias field to develop during cooling below T_C. However, in this work, attention should be paid to the fact that the internal bias field survives well above T_C. This means that, for an induced built-in bias field to be stable even above T_C, it should be free from the crystal symmetry because an internal bias field still exists at a cubic phase, which contradicts the symmetry-conforming defect dipole model.

A clue to overcoming this challenge was given by our recent work demonstrating that the spontaneous polarization of a textured ceramic can be forced to be aligned in the presence of an artificially generated bias field arising from included aligned ferroelectric templates, T_C of which exceeds that of the matrix ferroelectric ceramic [28]. A similar idea was suggested by incorporating semiconducting inclusions into polycrystalline piezoelectric ceramics as a 0−3 type composite, which improved their thermal stabilities with the existence of charges in the inclusions to compensate depolarization fields and thus maintained a poled state up to much higher temperatures [20,21]. However, their electromechanical properties are eventually depolarized in case a temperature passes through their T_C, implying the material must be repoled once it is heated above the T_C.

When MgO is added excessively, it is known that MgO-based fluid inclusions are frequently trapped inside growing PMNT single crystals because they are chemically inert [29,30]. Such fluid inclusions, commonly called negative crystals, are known to take their shape as the equilibrium shape of the encompassing crystal [30,31]. Therefore, the trapped fluid inclusions tend to be aligned preferentially sharing the same crystallographic orientations with the encompassing crystal. This means that they can play a role as serially connected charge collectors because the surfaces of MgO-based inclusions (MBIs) are non-polar but ionic [32−34]. In this work, we present a strategy for realizing mass-producible perpetually self-polarizing Mn-doped 0.71 $Pb(Mg_{1/3}Nb_{2/3})O_3$-0.29$PbTiO_3$ (Mn-PMNT) single crystals, once they are grown in the presence of excess MgO and B_2O_3 by a top-seeded solid-state crystal growth method (Fig. 1). It should be noted that these so-called self-poling effects are highly repeatable and stable after several heat treatments above their T_C, and such self-polarized phenomena are retained even after annealing at much higher temperatures such as 700 °C (Fig. S1) as well as repeated electrical cycling at high frequencies (Fig. S2).

2. Experimental section

2.1. Sample preparation

(001)-oriented pristine 0.71 $Pb(Mg_{1/3}Nb_{2/3})O_3$-0.29$PbTiO_3$ (abbreviated as $PMNT_{MBI}$) and a series of Mn-doped 0.71 $Pb(Mg_{1/3}Nb_{2/3})O_3$-0.29$PbTiO_3$ (0.1% (in mole) Mn doped case is specifically abbreviated as Mn-$PMNT_{MBI}$) single crystals were prepared into a thickness mode (k_t = 3.0 mm × 3.0 mm×0.5 mm) by a solid-state single crystal growth (SSCG) method (Ceracomp, Cheonan, South Korea). A large number of samples can be obtained from a large piece of as-grown crystals (Fig. 1b). One of the greatest advantages of the SSCG method is the compositional homogeneity that guarantees minimal fluctuation in the material properties as long as the pieces come from the same large piece [35]. To ensure the reproducibility of the self-poling effect in Mn-$PMNT_{MBI}$, we tested over 10 crystal pieces and confirmed their self-poling effect. We have also confirmed that the self-poling effect is consistently exhibited even after at least 20 cycles of heat treatment (Fig. S3). Pb_3O_4 (99.9%, Alfa Aesar, Ward Hill, MA), $MgNb_2O_6$ (99.9%, H. C. Starck GmbH, Newton, MA), and TiO_2 (99.99%, Ishihara, San Francisco, CA) were used as raw powder for the pristine $PMNT_{MBI}$. In Mn-$PMNT_{MBI}$, Columbite $Mg_{1-x}Mn_xNb_2O_6$ was prepared for the Mn ions to intendedly substitute the Mg ions to ensure the incorporated Mn to be donor or at least isovalent dopant. The Boron oxide compound was added for the sintering aids. Detailed sample preparations can be found elsewhere [25]. The crystal structure of powders and crystals was verified using X-ray diffraction (XRD: D8 ADVANCE, Bruker AXS, USA) with $Cu_{K\alpha}$ radiation (Fig. S4). The valences of incorporated Mn dopants were determined by X-ray photoelectron spectroscopy (XPS: K-alpha, ThermoFisher, USA). The spectra were fitted with three peaks at 641.2, 642.2 eV, and 644.4 eV, which corresponded to the valence of Mn^{2+}, Mn^{3+}, and Mn^{4+}, respectively (Fig. 1c). The gold electrode was sputtered on the (001) faces of platelet single crystals for electrical and electromechanical property measurements. Scanning electron microscopy (SEM) and electron backscattered diffraction (EBSD) image was gained by high-resolution energy dispersive spectroscopy (HREDS, Oxford instruments NanoAnalysis, Ultim Max 170). Based on the SEM images, we identified the well-developed facets of boron-rich MgO-based inclusions in comparison with pores and boron-deficient inclusions that had a round-shaped configuration or an irregular pattern. In the SEM images, we observed several pores that commonly exist in SSCG crystals. One should pay attention to the fact that pores can be minimized using an advanced sintering technique such as hot-pressing. However, it has been shown that the increase in the density by removing such pores was ineffective in increasing piezoelectric properties. More importantly, even in the presence of such large pores, the SSCG crystals still show as good piezoelectric and dielectric properties as the other crystals grown by a melting-involved growth technique (Table S1). More importantly, one of the best piezoelectric properties was reported in donor-doped single crystals grown by an SSCG method [36]. All

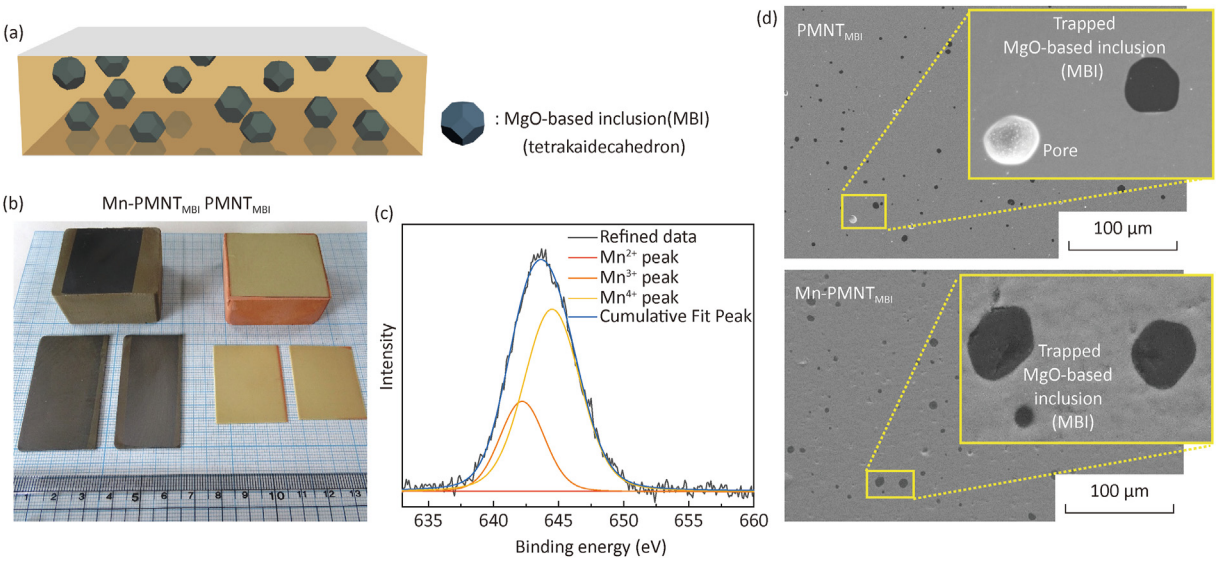

Fig. 1. (a) Schematic illustration of $PMNT_{MBI}$ and Mn-$PMNT_{MBI}$ single crystals forming a 0–3 composite. (b) As-grown and machined pristine $PMNT_{MBI}$ and Mn-$PMNT_{MBI}$ single crystals. (c) X-ray photoelectron spectroscopy (XPS) for the Mn 2p orbital of the Mn-$PMNT_{MBI}$ single crystal. (d) Typical microstructure images of the (001) surface of the $PMNT_{MBI}$ and Mn-$PMNT_{MBI}$ single crystals.

these imply that the correlation between the porosity and the piezoelectric properties has to be better clarified as a future investigation.

2.2. Dielectric, piezoelectric, and ferroelectric measurements

For DC-poling, a DC electric field was applied to samples with an amplitude of 10 kV/cm for 300 s at a poling temperature of 20 °C. The crystals were always annealed at 300 °C for 10 min before all poling processes with shorted top and bottom electrodes. After achieving a poled state, including self-poling, piezoelectric coefficients (d_{33}) were measured using a quasi-static piezo d_{33} m (YE2730, SINOCERA, China) at room temperature. For polarization hysteresis loops, a bipolar triangle electric field was applied to samples with an amplitude of 15 kV/cm, a frequency of 1–50 Hz, a cycle number of 1–20,000 and a temperature of 20–200 °C using a ferroelectric measurement system (aixPES, aixACCT, Germany).

The temperature-dependent dielectric permittivity ($\varepsilon^T_{33}/\varepsilon_0$) curves were measured in a customized furnace with an impedance/gain-phase analyzer (HP4194A, Agilent, USA) with an amplitude of 0.5 V, a frequency of 1 kHz–10 MHz and a temperature of 20–200 °C. Impedance spectra were also obtained by the same impedance/gain-phase analyzer in a range of 1 kHz–10 MHz with an amplitude of 1 V and a temperature of 20–200 °C. Electromechanical coupling factors for thickness mode (k_t) were calculated based on impedance spectra using the same impedance analyzer at a room temperature. The poling and depoling currents during thermal cycles were obtained in a customized furnace with a picoammeter (Keithley 487, Keithley, USA) with a temperature of 20–200 °C.

3. Results and discussion

To avoid any possible confusion regarding the crystal notation, we denote our PMNT crystals with a subscript MBI because all the PMNT single crystals used in this study include MBIs in the form of a 0–3 composite (Fig. 1a), *i.e.*, the PMNT single crystal and Mn-doped PMNT single crystal as $PMNT_{MBI}$ and Mn-$PMNT_{MBI}$, respectively. The MBI subscript indicates that the boron-rich MgO-based inclusions are distributed within the PMNT and Mn-PMNT matrix. One of the most readily identified signatures for the incorporation of Mn ions into the PMNT lattice is the change in the color as depicted in Fig. 1b–*i.e.*, from a desaturated dark yellow to a very dark grayish yellow. It is well-known that the changes in the color center are accompanied by a disturbance in the existing crystal field due to the formation of point defects. Given that Mn ions were introduced in the form of $MnNb_2O_6$ by replacing $MgNb_2O_6$ (Fig. S5), they are expected to be isovalent substitutes. However, X-ray photoelectron spectroscopy (XPS) on Mn 2p orbital revealed that most Mn^{2+} were transformed largely into Mn^{3+} and partly into Mn^{4+}, causing the major point defects to be cation vacancies; thus, the substituted Mn ions are mostly donors (Fig. 1c).

Fig. 1d is scanning electron micrographs of pristine $PMNT_{MBI}$ and Mn-$PMNT_{MBI}$, both of which exhibit trapped and dispersed boron-rich MBIs with well-developed faceted interfaces compared with the pores and the boron-deficient inclusions that have a round-shaped configuration or an irregular pattern (Fig. S6). Interestingly, all the trapped MBIs are nicely arrayed crystallographically, though what enabled such excellent alignment to be possible is not clear yet (Figs. S7 and S8). The function of boron-rich MBIs, which serve as the primary mechanism for self-polling by forming the 0–3 composite with a single crystal, will be elaborated on later.

Fig. 2a is a comparative presentation of the room-temperature polarization hysteresis loop of $PMNT_{MBI}$ and Mn-$PMNT_{MBI}$ with different levels of Mn doping. One can see that the magnitude of the internal bias field increases rapidly when the amount of Mn increases. Interestingly, the development of the internal bias field is an additive to the existing polarization state of the pristine $PMNT_{MBI}$ in that only the positive side of the coercive field increases with the increasing Mn content. Our study revealed that the internal bias field reaches its maximum value of 1.0 kV/cm when the doping level reaches 1.0% (in atomic) (Fig. 2b). Further increases in the doping level started to deteriorate the functional properties, though the magnitude of the internal bias field remained practically the same; therefore, we focus only on Mn-$PMNT_{MBI}$ with 1.0% Mn doping in this contribution.

Though considerably small, the pristine $PMNT_{MBI}$, as well as

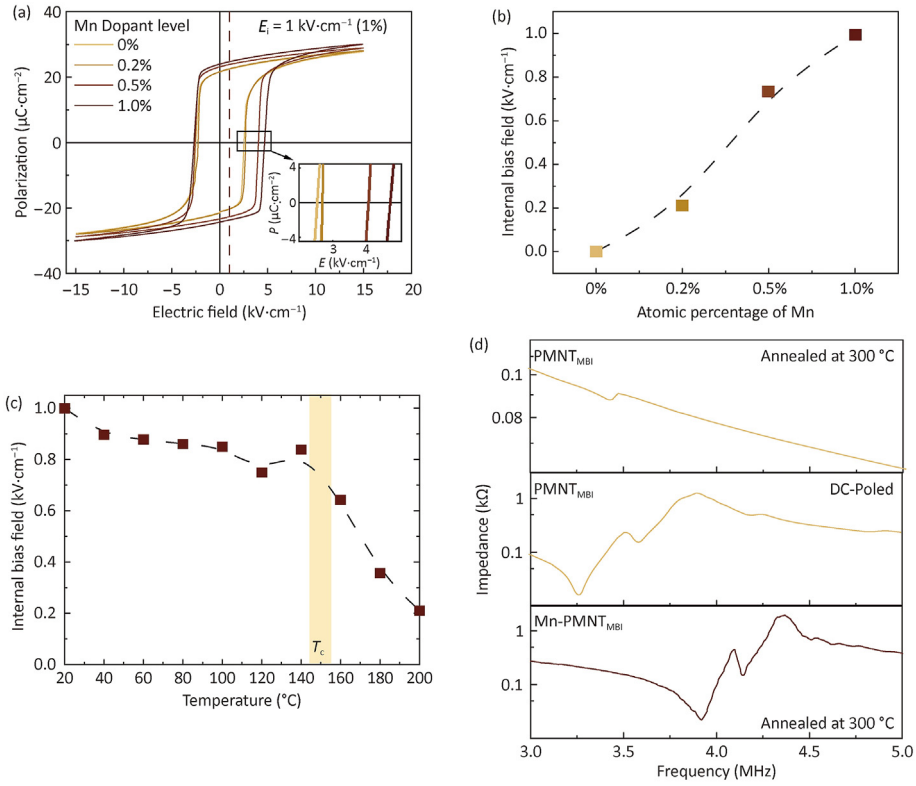

Fig. 2. (a) Room-temperature polarization hysteresis loops and (b) calculated internal bias field of the $PMNT_{MBI}$ and Mn-$PMNT_{MBI}$ as a function of doping level. (c) Change in the internal bias field as a function of temperature. (d) Impedance spectroscopy of the $PMNT_{MBI}$ measured at room temperature right after being thermally annealed at 300 °C (above T_C), DC-Poled $PMNT_{MBI}$, and Mn-$PMNT_{MBI}$ measured at room temperature right after being thermally annealed at 300 °C.

0.2% doped Mn-$PMNT_{MBI}$, also exhibits an internal bias field of 0.2 kV/cm, which is consistent with the presence of a trace of a vibration mode. Given that such an internal bias field is typically formed when acceptor-oxygen vacancy defect associates are generated by incorporating acceptor dopants [27], the observed internal bias field by Mn as a donor is unusual. Furthermore, we observed that the internal bias field was maintained preferentially along the [001] direction even above 200 °C that is more than 50 °C above T_C (Fig. 2c). We can say that the observed internal bias field has a different origin from that formed by the usual acceptor-oxygen vacancy defect dipoles. Since acceptor-oxygen vacancy defect dipoles should conform to the given crystal symmetry [27,37], they have no preferential crystallographic directionality when the macrosymmetry of crystals is cubic.

It is well-known that as-prepared ferroelectrics are in a multi-domain state, meaning that macroscopic net polarization is zero. Therefore, as-prepared specimens must be electrically poled along a certain crystallographic direction by applying an external electric field for the inherent piezoelectricity to be activated. However, Mn-$PMNT_{MBI}$ is already piezoelectrically active even in its as-prepared state, evident from the presence of a multitude of vibration modes (Fig. 2d). It is noted that the impedance spectrum stays practically the same before and after poling treatment, while it changes dramatically in the pristine $PMNT_{MBI}$. A detailed list of material properties of self-poled Mn-$PMNT_{MBI}$ single crystals is provided in Table S1 in comparison with other single crystals grown by melting-involved growth techniques.

Fig. 3a depicts the change in the charging state of electrically poled $PMNT_{MBI}$ and Mn-$PMNT_{MBI}$, measured during a thermal cycle, *i.e.*, heating up to 200 °C and a subsequent cooling back to room temperature. As noted, electrical poling treatment induces a macroscopic net polarization state by aligning the initially randomly oriented local polarization vectors through current injection onto the electrodes. This means that any loss in the net polarization state leads to a current flow out of the specimen. Two outbound current flows are denoted in the poled $PMNT_{MBI}$ during heating, which is typical for relaxor-PT crystals. About 80% of the polarization state is lost across T_{R-T}, and the rest passes T_C. As naturally expected, this type of thermal cycle completely depoles $PMNT_{MBI}$ with no chance for the lost polarization to be recovered during subsequent cooling in the absence of an external electric field since there is no driving force for aligning polarization elements along any specific orientations.

The temperature-dependent polarization state of Mn-$PMNT_{MBI}$ during a thermal cycle shows a unique behavior. We note three distinct features. One is that T_{R-T}, which is commonly known as a phase transformation temperature between a low-temperature rhombohedral and a high-temperature tetragonal phase, unexpectedly increases the polarization state during heating, indicating that the spontaneous polarization is aligned by itself. Another is that the lost polarization recovers itself up to ~90% even in the absence of an external electric field during cooling (The detailed process of calculating polarization from temperature-dependent current measurements can be found in Fig. S9). This recovery is also observed in the piezoelectric coefficient, which can be noticed in Fig. 3b, and it has been confirmed to persist even after performing repeated thermal cycles. The 10% degradation is seen to be related to a partial depoling across T_{R-T} during cooling, which again strongly suggests that the internal bias field is not associated with the crystal symmetry but fixed along the [001] direction. Finally, despite the fact that relaxor-$PbTiO_3$ single crystals are known to possess relaxor characteristics [38], Mn-$PMNT_{MBI}$ single crystals

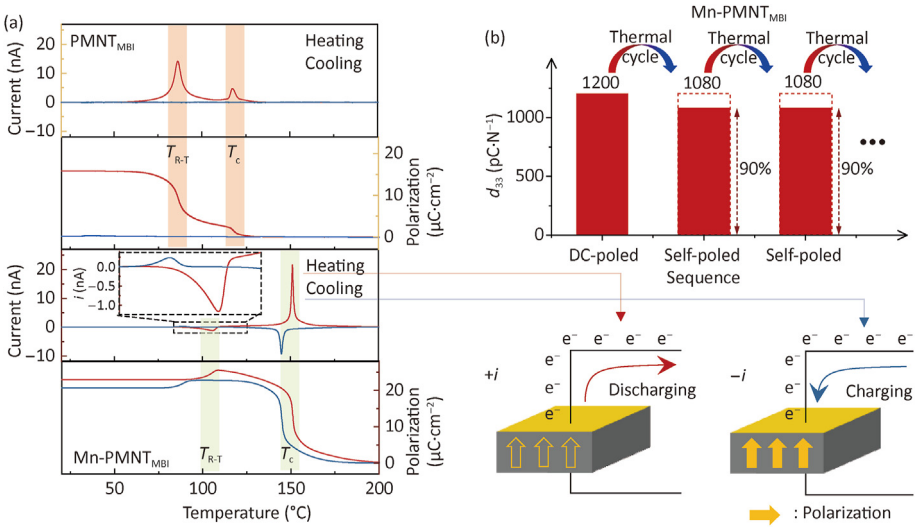

Fig. 3. (a) A comparative current measurement and the consequent changes in the polarization state of poled PMNT$_{MBI}$ and Mn-PMNT$_{MBI}$ measured during a thermal cycle up to 200 °C. During the heating process (the red arrow), the pre-existing long-range ordered polarization (the solid yellow arrows) disappears as it passes through T_c. Then, during the cooling process (the blue arrow), starting around 180 °C, Mn-PMNT$_{MBI}$ begins to be poled again, resulting in the re-emergence of the long-range ordered polarization (the hollow yellow arrows). (b) Graph representing the change in the piezoelectric coefficient of Mn-PMNT$_{MBI}$ single crystal according to the heat treatment cycle.

behave like normal ferroelectrics and hence show a first-order phase transformation at so-called T_{R-T}, whereas PMNT$_{MBI}$ single crystals do not show any peaks regarding phase transformations in the vicinity of T_{R-T} during cooling. We deduce that such a transition from relaxor ferroelectrics to normal ferroelectrics is attributed to the existence of the internal bias field, making polar entities of the former transformed into long-range ordered ferroelectric phases of the latter.

To understand the underlying mechanism for the observed self-poling, we quenched Mn-PMNT$_{MBI}$ crystal from 300 °C, at which the crystal is close to a paraelectric cubic. As shown in Fig. 4a, no piezoelectric vibration mode is discerned in the impedance spectrum of the quenched Mn-PMNT$_{MBI}$, meaning that an unpoled state is induced by the quenching. Hence, the net polarization of the quenched crystal is close to zero. Temperature-dependent dielectric permittivity of the quenched crystal is presented in Fig. 4b in comparison with that of both DC-poled PMNT$_{MBI}$ and self-poled Mn-PMNT$_{MBI}$. One can see that the shape profile of quenched Mn-PMNT$_{MBI}$ is similar to that of DC-poled PMNT$_{MBI}$, *i.e.*, two successive increases in the permittivity values at T_{R-T} and T_c. On the contrary, the dielectric permittivity of self-poled Mn-PMNT$_{MBI}$ drops at T_{R-T}, resulting from the reduction in the domain walls due to domain growth, *i.e.*, poling (a poling current is detected at T_{R-T}, Fig. 3), in the presence of the [001]-oriented internal bias field.

Attention needs to be paid to the fact that Mn-PMNT$_{MBI}$ is unpoled by the quenching treatment poles of itself during heating across T_{R-T}, as manifested in Fig. 4c. As noted, T_{R-T} is commonly referred to as the temperature where the low-temperature rhombohedral is transformed into the high-temperature tetragonal symmetry. Considering some polarization switching of spontaneous polarization vectors from <111> to [001] or [00 $\bar{1}$] direction at T_{R-T}, one may expect that at least a partial self-poling should have been induced in the quenched Mn-PMNT$_{MBI}$ at T_{R-T} during a heat cycle (Fig. S10). Furthermore, the fact that the suppressed self-poling state by the quenching treatment was reactivated simply by heating up the specimen to the high-temperature regime suggests that the [001]-oriented internal bias field should develop simultaneously with the appearance of spontaneous polarization accompanied by a long-range order. This conclusion is well-supported by the observation that the internal bias field can still

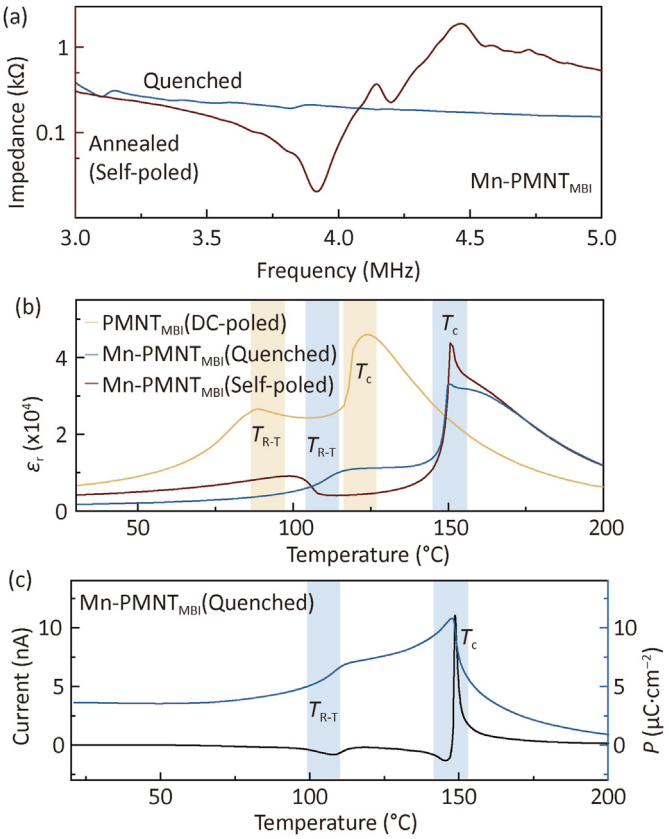

Fig. 4. (a) Frequency sweep of the impedance of the Mn-PMNT$_{MBI}$, furnace-cooled and quenched after being thermally annealed at 300 °C. (b) Comparative temperature-dependent dielectric permittivity of the self-poled and quenched Mn-PMNT$_{MBI}$ in reference to the DC-poled PMNT$_{MBI}$. (c) Current measurement on the quenched Mn-PMNT$_{MBI}$ during heating.

be induced in response to an external electric field, even when the net spontaneous polarization is absent as the crystal is heated up above T_C. (Fig. 2c).

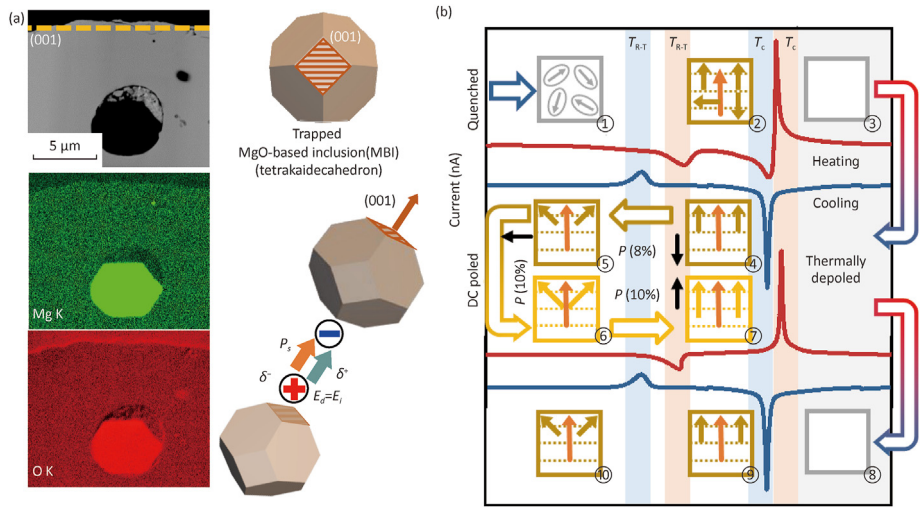

Fig. 5. (a) Backscattered electron image and energy-dispersive spectroscopy mapping images of a MBI in the view of the perpendicular surface to (001). (b) A schematic illustration of the changes in the polarization states after a quenching treatment, followed by two successive thermal annealing treatments.

As previously stated, the boron-rich MBI with well-developed faceted interfaces can be observed to be closely aligned with the (001) surface. The facets were identified as $\{100\}_{pc}$ and $\{111\}_{pc}$ (the subscript 'pc' denotes pseudocubic indices), as visualized in Fig. 5a. A statistical analysis (Fig. S11) on the shape of the included MBIs enables us to model them to be a tetrakaidecahedron composed of six $\{100\}_{pc}$ and eight $\{111\}_{pc}$ planes. The appearance of spontaneous polarization along the [001] direction is mediated by an internal bias field formed by the Mn-induced space charges segregating at the $\{100\}_{pc}$ planes of MBIs. As noted, the $\{100\}_{pc}$ surfaces of MBIs terminate discretely with the ionic species of Mg^{2+} and O^{2-}; thus, the surface can easily accommodate charged species [32–34,39–41]. This means that once the amount of mobile charges is large enough in the system, any electric field induced by the development of a spontaneous polarization could force the mobile charges to migrate towards the $\{100\}_{pc}$ surfaces of MBIs, giving rise to the appearance of an electric field that counterbalances the local electric field originating from the spontaneous polarization, which makes the origin for the self-poling even in the absence of an external electric field. What we have discussed so far is summarized with a schematic illustration in Fig. 5b. Furthermore, our arguments are also supported by a self-poling effect of [110]-oriented single crystals wherein a net polarization generated by self-poling, *i.e.* [001]-oriented internal bias field, should be less than [001]-oriented single crystals according to mathematical calculations (Figs. S12 and S13).

4. Conclusions

The Mn-$PMNT_{MBI}$ single crystals were prepared by a solid-state crystal growth method (SSCG). They exhibited a spontaneous self-alignment of polarizations during cooling through T_C, *i.e.*, self-poling. Temperature-dependent current measurements and calculated polarization variations during thermal cycles identified space charge-induced local electric field counter-balancing the spontaneous polarization inherent to the crystal as the driving force for self-poling. The piezoelectric coefficient of self-poled crystals reached about 90% of the value achieved by DC-poling at room temperature due to a partial depoling across the so-called $T_{R\text{-}T}$. Given that the thermal stability of piezoelectric materials in terms of both working environments and self-heating during operation is a ceaseless concern to the device engineers, we expect that the currently reported perpetually self-activating piezoelectricity has an unprecedented impact on the piezoelectric industry.

CRediT authorship contribution statement

Hwang-Pill Kim: Data curation, Formal analysis, Writing – original draft. **Geon-Ju Lee:** Data curation, Formal analysis, Investigation, Methodology. **Ju-Hyeon Lee:** Data curation, Methodology, Visualization, Writing – review & editing. **Jae-Hyeon Cho:** Visualization. **Hye-Lim Yu:** Methodology. **Woo-Seok Kang:** Methodology. **Joo-Hee Kang:** Methodology. **Ho-Yong Lee:** Methodology. **Wook Jo:** Conceptualization, Formal analysis, Writing – review & editing.

Declaration of competing interest

The authors declare that they have no known competing financial interests or personal relationships that could have appeared to influence the work reported in this paper.

Acknowledgments

This work was supported by the Technology Innovation Program funded by the Ministry of Trade, Industry & Energy (MOTIE, Korea) (20022441). JHK was supported by the Fundamental Research Program of Korea Institute of Materials Science (PNKA170).

Appendix A. Supplementary data

Supplementary data to this article can be found online at https://doi.org/10.1016/j.jmat.2024.05.002.

References

[1] MarketsandMarkets. Piezoelectric devices market with COVID-19 impact analysis by material (piezoelectric ceramics, polymers), product (piezoelectric actuators, transducers, motors). Application (Aerospace & Defense, Industrial, Consumer), and Region - Global Forecast to 2026; 2021.
[2] Zhou Q, Lam KH, Zheng H, Qiu W, Shung KK. Piezoelectric single crystal ultrasonic transducers for biomedical applications. Prog Mater Sci 2014;66:87–111.
[3] Zhang S, Li F, Jiang X, Kim J, Luo J, Geng X. Advantages and challenges of relaxor-$PbTiO_3$ ferroelectric crystals for electroacoustic transducers – a review. Prog Mater Sci 2015;68:1–66.
[4] Priya S, Song H-C, Zhou Y, Varghese R, Chopra A, Kim S-G, et al. A review on piezoelectric energy harvesting: materials, methods, and circuits. Energy

Harvest Syst 2017;4:3–39.
[5] Randall CA, Kelnberger A, Yang GY, Eitel RE, Shrout TR. High strain piezoelectric multilayer actuators—a material science and engineering challenge. J Electroceram 2005;14:177–91.
[6] Rödel J, Webber KG, Dittmer R, Jo W, Kimura M, Damjanovic D. Transferring lead-free piezoelectric ceramics into application. J Eur Ceram Soc 2015;35:1659–81.
[7] Park S-E, Shrout TR. Ultrahigh strain and piezoelectric behavior in relaxor based ferroelectric single crystals. J Appl Phys 1997;82:1804–11.
[8] Shrout TR, Chang ZP, Kim N, Markgraf S. Dielectric behavior of single crystals near the $(1-x)Pb(Mg_{1/3}Nb_{2/3})O_3$-$(x)PbTiO_3$ morphotropic phase boundary. Ferroelectr, Lett Sect 1990;12:63–9.
[9] Liu X, Tan P, Ma X, Wang D, Jin X, Liu Y, et al. Ferroelectric crystals with giant electro-optic property enabling ultracompact Q-switches. Science 2022;376:371–7.
[10] Sun E, Cao W. Relaxor-based ferroelectric single crystals: growth, domain engineering, characterization and applications. Prog Mater Sci 2014;65:124–210.
[11] Qiu C, Wang B, Zhang N, Zhang S, Liu J, Walker D, et al. Transparent ferroelectric crystals with ultrahigh piezoelectricity. Nature 2020;577:350–4.
[12] Höfling M, Zhou X, Riemer LM, Bruder E, Liu B, Zhou L, et al. Control of polarization in bulk ferroelectrics by mechanical dislocation imprint. Science 2021;372:961–4.
[13] Kalinin SV, Rodriguez BJ, Borisevich AY, Baddorf AP, Balke N, Chang HJ, et al. Defect-mediated polarization switching in ferroelectrics and related materials: from mesoscopic mechanisms to atomistic control. Adv Mater 2010;22:314–22.
[14] Li F, Lin D, Chen Z, Cheng Z, Wang J, Li C, et al. Ultrahigh piezoelectricity in ferroelectric ceramics by design. Nat Mater 2018;17:349–54.
[15] Li F, Zhang S, Yang T, Xu Z, Zhang N, Liu G, et al. The origin of ultrahigh piezoelectricity in relaxor-ferroelectric solid solution crystals. Nat Commun 2016;7:13807.
[16] Weyland F, Acosta M, Koruza J, Breckner P, Rödel J, Novak N. Criticality: concept to enhance the piezoelectric and electrocaloric properties of ferroelectrics. Adv Funct Mater 2016;26:7326–33.
[17] Li J, Shen Z, Chen X, Yang S, Zhou W, Wang M, et al. Grain-orientation-engineered multilayer ceramic capacitors for energy storage applications. Nat Mater 2020;19:999–1005.
[18] Saito Y, Takao H, Tani T, Nonoyama T, Takatori K, Homma T, et al. Lead-free piezoceramics. Nature 2004;432:84–7.
[19] Yang S, Li J, Liu Y, Wang M, Qiao L, Gao X, et al. Textured ferroelectric ceramics with high electromechanical coupling factors over a broad temperature range. Nat Commun 2021;12:1414.
[20] Zhang J, Pan Z, Guo F-F, Liu W-C, Ning H, Chen Y, et al. Semiconductor/relaxor 0–3 type composites without thermal depolarization in $Bi_{0.5}Na_{0.5}TiO_3$-based lead-free piezoceramics. Nat Commun 2015;6:6615.
[21] Zhao C, Gao S, Yang T, Scherer M, Schultheiß J, Meier D, et al. Precipitation hardening in ferroelectric ceramics. Adv Mater 2021;33:2102421.
[22] Li F, Cabral MJ, Xu B, Cheng Z, Dickey EC, LeBeau JM, et al. Giant piezoelectricity of Sm-doped $Pb(Mg_{1/3}Nb_{2/3})O_3$-$PbTiO_3$ single crystals. Science 2019;364:264–8.
[23] Kim H-P, Ahn CW, Hwang Y, Lee H-Y, Jo W. Strategies of a potential importance, making lead-free piezoceramics truly alternative to PZTs. J Korean Ceram Soc 2017;54:86–95.
[24] Luo L, Li W, Zhu Y, Wang J. Growth and characteristics of Mn-doped PMN–PT single crystals. Solid State Commun 2009;149:978–81.
[25] Oh H-T, Joo H-J, Kim M-C, Lee H-Y. Thickness-dependent properties of undoped and Mn-doped (001) PMN-29PT $[Pb(Mg_{1/3}Nb_{2/3})O_3$-$29PbTiO_3]$ single crystals. J Korean Ceram Soc 2018;55:290–8.
[26] He C, Wang Z, Li X, Yang X, Long X, Ye Z-G. Self-polarized high piezoelectricity and its memory effect in ferroelectric single crystals. Acta Mater 2017;125:498–505.
[27] Ren X. Large electric-field-induced strain in ferroelectric crystals by point-defect-mediated reversible domain switching. Nat Mater 2004;3:91–4.
[28] Ahn CW, Choi G, Kim IW, Lee J-S, Wang K, Hwang Y, et al. Forced electrostriction by constraining polarization switching enhances the electromechanical strain properties of incipient piezoceramics. NPG Asia Mater 2017;9.e346–e346.
[29] Jo W, Chung U-J, Hwang N-M, Kim D-Y. Effect of SiO_2 and TiO_2 addition on the morphology of abnormally grown large $Pb(Mg_{1/3}Nb_{2/3})O_3$–35mol% $PbTiO_3$ grains. J Am Ceram Soc 2005;88:1992–4.
[30] Joo-Hwan H, Young-Keun C, Doh-Yeon K, Sang-Hee C, Yoon DN. Temperature dependence of the shape of ZnO grains in a liquid matrix. Acta Metall 1989;37:2705–8.
[31] Chatain D, Wynblatt P, Rohrer GS. Equilibrium crystal shape of Bi-saturated Cu crystals at 1223 K. Acta Mater 2005;53:4057–64.
[32] Chen H-YT, Giordano L, Pacchioni G. From heterolytic to homolytic H_2 dissociation on nanostructured MgO (001) films as a function of the metal support. J Phys Chem C 2013;117:10623–9.
[33] Pacchioni G, Freund H. Electron transfer at oxide surfaces. The MgO paradigm: from defects to ultrathin films. Chem Rev 2013;113:4035–72.
[34] Prada S, Giordano L, Pacchioni G. Li, Al, and Ni substitutional doping in MgO ultrathin films on metals: work function tuning via charge compensation. J Phys Chem C 2012;116:5781–6.
[35] Kang SJL, Park JH, Ko SY, Lee HY. Solid-state conversion of single crystals: the principle and the state-of-the-art. J Am Ceram Soc 2015;98:347–60.
[36] Kim H-P, Wan H, Luo C, Sun Y, Yamashita Y, Karaki T, et al. A review on alternating current poling for perovskite relaxor-$PbTiO_3$ single crystals. IEEE Trans Ultrason Ferroelectrics Freq Control 2022;69:3037–47.
[37] Arlt G, Neumann H. Internal bias in ferroelectric ceramics: origin and time dependence. Ferroelectrics 1988;87:109–20.
[38] Kim H-P, Lee G-J, Jeong HY, Jang J-H, Kim G-Y, Choi S-Y, et al. Symmetry-bridging phase as the mechanism for the large strains in relaxor-$PbTiO_3$ single crystals. J Eur Ceram Soc 2019;39:3327–31.
[39] Nigam S, Majumder C. Charge reordering of MgO (100) surface by Sn cluster deposition: implications for heterogeneous catalysis. Appl Surf Sci 2020;506:144963.
[40] Mammen N, de Gironcoli S, Narasimhan S. Substrate doping: a strategy for enhancing reactivity on gold nanocatalysts by tuning sp bands. J Chem Phys 2015;143:144307.
[41] Farmer JA, Ruzycki N, Zhu JF, Campbell CT. Lithium adsorption on MgO (100) and its defects: charge transfer, structure, and energetics. Phys Rev B 2009;80:035418.

Hwang-Pill Kim is a senior researcher at the Agency for Defense Development (ADD), Republic of Korea. He received his B.S. and Ph.D. degrees in Materials Science and Engineering from the Ulsan National Institute of Science and Technology (UNIST), Republic of Korea. From 2021 to 2023, he joined North Carolina State University as a postdoctoral fellow. pollux345@naver.com

Geon-Ju Lee is a researcher at MLCC Composition Lab, Component Biz. Unit, Samsung Electro Mechanics Co. Ltd., Suwon 16674, Republic of Korea. He received his Ph.D. degree in Materials Science and Engineering from the Ulsan National Institute of Science and Technology (UNIST), Republic of Korea. gjlee@unist.ac.kr

Wook Jo is a professor at the Ulsan National Institute of Science and Technology (UNIST), Republic of Korea. He received his Ph.D. degree in Materials Science and Engineering at Seoul National University, Republic of Korea. His research interests are ferroelectric ceramics, dielectric materials, oxide catalysts, room-temperature single-phase multiferroics, transparent piezoceramics, and textured ceramics. wookjo@unist.ac.kr